Journal Article

Impact of cod skin peptide-ι-carrageenan conjugates prepared via the Maillard reaction on the physical and oxidative stability of Antarctic krill oil emulsions

Han, L., Zhai, R., Shi, R., Hu, B., Yang, J., Xu, Z., Ma, K., Li, Y. and Li, T.

Recommended citation:

Impact of cod skin peptide-ι-carrageenan conjugates prepared via the Maillard reaction on the physical and oxidative stability of Antarctic krill oil emulsions
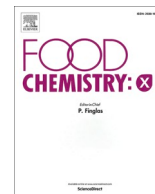
Lingyu Han [a,1], Ruiyi Zhai [a,1], Ruitao Shi [a], Bing Hu [a], Jixin Yang [b], Zhe Xu [a], Kun Ma [a], Yingmei Li [c], Tingting Li [a,*]

[a] *Key Lab of Biotechnology and Bioresources Utilization of Ministry of Education, College of Life Science, Dalian Minzu University, Dalian, Liaoning 116600, China*
[b] *Faculty of Arts, Science and Technology, Wrexham Glyndwr University, Plas Coch, Mold Road, Wrexham LL11 2AW United Kingdom*
[c] *Linghai Dalian Seafoods Breeding Co., Ltd, Jinzhou, Liaoning 121209, China*

ARTICLE INFO

ABSTRACT

This research aimed to construct an emulsifier by the Maillard reaction at various times using cod fish skin collagen peptide (CSCP) and ι-carrageenan (ι-car) to stabilize an Antarctic krill oil (AKO) emulsion. This emulsion was then investigated for physicochemical stability, oxidative stability, and gastrointestinal digestibility. The emulsion stability index and emulsifying activity index of Maillard reaction products (MRPs) were increased by 36.32 % and 66.30 %, respectively, at the appropriate graft degree (25.58 %) compared with the mixture of ι-car and CSCP. In vitro digestibility suggested the higher release of free fatty acids (FFAs) of 10d-MRPs-AKO-emulsion, and the highest bioavailability of AST in 10d-MRPs-AKO was found to be 28.48 %. The findings of this study showed the potential of MRPs to improve peptide function, serve as delivery vehicles for bioactive chemicals, and possibly serve as a valuable emulsifier to be used in the food industry.

1. Introduction

Antarctic krill oil (AKO) is rich in phospholipids (PLs), ω-3 polyunsaturated fatty acids (ω-3 PUFAs), vitamins, minerals, astaxanthin (AST), and flavonoids (Xie et al., 2019). In addition to being an essential nutrient, long chain ω-3 PUFAs have been shown to have positive health impacts, including anti-inflammatory, antithrombotic, antiarrhythmic, and antiatherosclerotic effects (Bakry et al., 2016; Olmedo, Nepote, & Grosso, 2014). Because of its antioxidant properties, AST is a highly valued biomolecule, although it is highly sensitive to degradation (Sánchez, Zavaleta, García, Solano, & Díaz, 2021). However, oils enriched in PUFAs are especially vulnerable to the oxidative formation and degradation of undesirable flavours (El-Messery, Altuntas, Altin, & Özçelik, 2020). Hence, strategies are required to surmount the poor aqueous solubility and oxidative instability of AKO.

Emulsion technology is among the most efficient methods for increasing the stability and water dispersibility of polyunsaturated lipids. Emulsion stability is thought to be primarily affected by the emulsion's composition and structure, as well as the storage conditions.

Molecular and physicochemical mechanisms during lipid oxidation in multiphase systems must be understood for appropriate emulsion-based delivery system design. Hydroperoxides are formed when oxygen combines with unsaturated lipids during the initial stage of lipid oxidation; these molecules are amphiphilic and frequently accumulate at oil–water interfaces. This allows the hydroperoxides to interact with prooxidants in the surrounding aqueous phase, such as transition metals or hydrophilic compounds. The free radicals produced by this reaction can penetrate lipid droplets and initiate chain reactions involving additional lipids (Berton-Carabin, Ropers, & Genot, 2014; Wang, Sun, Lu, Gul, Mata, & Fang, 2020). Consequently, placing antioxidant emulsifiers at the droplet surfaces, where they can scavenge free radicals, may enhance the oxidative stability of AKO emulsions.

Antioxidants are used in food products to increase their stability, but typically, these are synthetic antioxidants. Because of customer preference, the need for natural antioxidants has increased over time. The productions of the Maillard reaction are an example of a natural antioxidant. A reducing sugar such as fructose or glucose reacts with the amino group of proteins, peptides, or amino acids to produce brown

---

melanoidins during the Maillard reaction, a natural nonenzymatic browning process in food occurring during thermal processing (Hwang, Kim, Woo, Lee, & Jeong, 2011). The antioxidant activity of Maillard reaction products (MRPs) of glucose and amino acids has been demonstrated through various processes, such as the scavenging of radicals and the chelation of metals (Maillard, Billaud, Chow, Ordonaud, & Nicolas, 2007; Morales & Babbel, 2002). Nagachinta and Akoh (2013) employed MRPs as an encapsulant derived from whey protein isolates corn syrup solids for a structured lipid human milk fat analogue with low thiobarbituric acid-reactive compounds (TBARS) and low peroxide values (PVs). It has been reported that glucose-cysteine MRPs are effective in lipophilic radical scavenging and possess chelating capacity; however, numerous potential sugar and amino acid combinations produce a natural antioxidant (Maillard, Billaud, Chow, Ordonaud, & Nicolas, 2007). Another study indicated that among all glucose and fructose-derived amino acids, glucose-cysteine MRPs had the best scavenging potential for 2,2′-azino-bis (3-ethylbenzothiazoline-6-sulfonic acid) (ABTS) and 2,2-diphenyl-1-picrylhydrazyl (DPPH) radicals (Hwang, Kim, Woo, Lee, & Jeong, 2011).

Hydrolysed collagen (known as collagen peptides) demonstrates a wide range of positive benefits, including antihypertensive and antidiabetic properties (Abdelhedi & Nasri, 2019). The raw materials used to form collagen peptides are often hides, skin, and bones derived from livestock and fish processing (Hong, Fan, Chalamaiah, & Wu, 2019). Because of its enormous economic worth, the Atlantic cod (*Gadus morhua L.*) is considered one of the world's most significant fish. Skin, which includes a high degree of collagen, is formed during industrial cod processing and is generally wasted or utilized to produce low-value products (Chen, Yang, Hong, Feng, Liu, & Luo, 2020). Underutilization of cod skin leads to a loss of potential profits and disposal costs. Therefore, recovering useful components, specifically collagen peptides, from cod skin is important from both an environmental and economic perspective. Kangni Chen prepared xylose-cod skin collagen peptide (xylose-CSCP) MRPs. The results showed that after 150 min of heating at 120 °C, the reduction power and ABTS scavenging activity of the xylose-CSCP MRPs were 0.887 absorbance units and 99.59 %, respectively.

The present study aims to investigate the effect of ι-carrageenan (ι-car) on the antioxidant properties and emulsion stability of cod skin collagen peptides (CSCP). Antioxidant emulsifiers were prepared in this study using the Maillard reaction via conjugation of cod skin collagen peptides (CSCP) with ι-carrageenan (ι-car). For this purpose, the CSCP and ι-car mixtures were first heated in the dry state under controlled Maillard reactions. To assess the extent of conjugation and structural alterations, the conjugates were subjected to FTIR spectroscopy, browning intensity, and fluorescence spectroscopy. Finally, the oxidative stability of the conjugate-stabilized emulsions was assessed by measuring peroxide values in the model system. The findings of this research may offer theoretical support for the potential of MRPs to enhance the physicochemical characteristics of CSCP and its ability to serve as a lipophilic biological transporter. Additionally, it may lead to a rise in the utilization rate of byproducts derived from cod processing.

2. Materials and methods

2.1. Materials and chemicals

CSCP and AKO were obtained from Binzhou Wanjia (Shandong, China) and Lu Hua Biological Technology Company (Shandong, China), respectively. ι-car was obtained from Yuanye Bio-Technology Co., Ltd. (Shanghai, China).

2.2. Preparation of MRPs

A uniform dispersion was formed by suspending CSCP and ι-car (1:4, m/m) in phosphate buffer (pH 7.0, 0.05 mmol/L) and stirring the mixture for 2 h, followed by freeze-drying. After drying the mixes, they were placed in a desiccator with a supersaturated KBr solution (79 % relative humidity) and incubated at 60 °C. After 0-2-4-6-8-10-12-14 days, samples were collected from each mixture and stored at −20 °C before use.

2.3. Molecular weight distribution

The experiment was carried out following the approach reported by Siewe, Kudre, Bettadaiah, and Narayan (2020) with some modifications. The gel-permeation chromatography with an Xtimate *SEC*-120 column (300 × 7.8 mm, 5 μm) based on an Elite P230 high-performance liquid chromatography (HPLC) system was used to determine the molecular weight (MW) distribution profiles of peroxides. 1 mg/mL solutions of samples, filtered through a 0.22 μm filter, were prepared, and 40 μL of each solution was loaded into the HPLC column. The mobile phase used was acetonitrile/water/trifluoroacetic acid in a ratio of 30:70:0.1 (v/v/v). The sample was eluted at a 0.5 mL/min flow rate. Using the following Sigma standards, a calibration curve for MW was constructed: cytochrome *C* (12384 Da), aprotinin (6511.44 Da), tetrapeptide (1072 Da), tetrapeptide GGYR (451.48 Da), and lysine (146.2 Da). The data were collected with a UV detector set at 214 nm.

The Eq. (1) shows the standard calibration curve obtained.

$$Y = -2740.70X + 42849.64 \, (R^2 = 0.9997) \tag{1}$$

where Y denotes the relative molecular weight of samples (MW), and X denotes the corresponding retention time.

2.4. Circular dichroism spectroscopy

Using a Jasco J-815 spectropolarimeter with a Peltier-controlled cell holder in a precision quartz cell of 1 mm path-length from 190 to 250 nm with a bandwidth of 0.1 nm and a scan speed of 20 nm·min^{-1}, CD spectra of CSCP (diluted 100-fold in Milli-Q water at pH 7.0) were collected at 20 °C. The spectra underwent background subtraction, were subjected to averaging over a total of 10 scans.

2.5. FTIR

A Nicolet 5700 FTIR spectrometer was used to determine the infrared spectra of the dried MRPs samples. A dried sample powder weighing 1 mg was mixed with KBr (100 mg) and subsequently ground using an agate mortar. The resulting mixture was then analysed at 4 cm^{-1} resolution with 32 scans over a range of 4000–400 cm^{-1}.

2.6. Determination of the degree of graft

The present study utilized the O-phthaldialdeyde (OPA) method, as described in the literature by Mao, Pan, Hou, Yuan, and Gao (2018) with minor alterations, to indirectly assess the degree of graft (DG) by analysing free amino groups. The freshly prepared OPA reagent was used, which was based on the following reagents: OPA (40 mg) was dissolved in a mixture of sodium borate buffer (0.1 mol/L, 25 mL, pH 9.85), methanol (1 mL), 20 % (w/v, 2.5 mL) SDS and β-mercaptoethanol (100 μL) in deionized water. The solution was subjected to dilution with water until a 50 mL volume was achieved. Briefly, 200 μL of sample solution and 4 mL of OPA were mixed in the tube and allowed to react for 2 min in a water bath at 35 °C. Using a UV-1800 spectrophotometer (Shimadzu, Japan), the absorbance of the reacting solution was immediately recorded at 340 nm. Lysine concentrations between 0.5 and 3 mmol/L were used to construct a calibration curve.

Eq. (2) was used to determine DG in terms of the relative increase or decrease in the availability of free amino groups.

$$DG = \frac{(C_0 - C_t)}{C_0} \times 100\% \tag{2}$$

where C_0 and C_t demonstrate the presence of free amino groups in the mixture before and after incubation, respectively.

2.7. Measurement of browning intensity

A UV–visible spectrophotometer (Model UV-2600A, UNICO, Shanghai, China) was used to assess the browning intensity of the 10 mg/ml sample by recording the absorbance at 420 nm.

2.8. Determination of fluorescence intensity

Dried samples were reconstituted at a dose of 0.02 mg/ml in phosphate buffer (pH 7.0, 10 mmol/L). Using a fluorescence spectrophotometer (F-7000, Hitachi, Japan), the fluorescence intensity of samples was recorded at 347 nm of an excitation wavelength and 370 nm to 650 nm of emission wavelengths, as described by Cao, Yan, and Liu (2022).

2.9. Determination of emulsifying capacity

The determination of the emulsifying potential of ι-car-CSCP MRPs was carried out by using the method described previously with some modifications (Ai, Xiao, & Jiang, 2021). Phosphate buffer (10 mmol/L, pH 7.0) was used to dilute the reaction sample to a concentration of 0.9 % (wt). After introducing the diluted sample to the AKO at a volume ratio of 5:95, the mixture was homogenized at room temperature using a T25 Easy clean disperser (IKA, Staufen, Germany) for 1 min at a speed of 20,000 rpm. At 0 and 10 min, 20 μL of the bottom sample was added to 4.98 mL of SDS solution (0.1 % w/v), followed by absorbance determination at 500 nm. The absorbance value obtained at 0 min and 10 min were referred to A_0 and A_{10}. The Eqs. (3) and (4) were used to determine emulsifying activity index (EAI) and emulsifying stability index (ESI)

$$EAI(m^2/g) = \frac{2 \times 2.303 \times A_0 \times dilution factor}{C \times \Phi \times 10^4} \quad (3)$$

$$ESI = \frac{A_0 \times 10}{A_0 - A_{10}} \quad (4)$$

where C is the initial concentration of MRPs (g/mL) and ϕ is the volume fraction of oil phase.

2.10. Antioxidant activity

DPPH radical scavenging properties assay

The DPPH radical scavenging activity (RSA) was determined using a modified version of the procedure described by Yu, He, Tang, Zhang, Zhu, and Sun (2018). DPPH solution (0.2 mmol/L in ethanol) was incorporated into the sample, i.e., MRPs solution (1 mg/ml) in equal proportion. Similarly, an equal proportion of ethanol was added to the sample solution serving as a control, while the blank was composed of a mixture of ethanol and DPPH solution in equal proportions. After that, the samples were incubated for 30 min in the dark, and the absorbance was recorded at 517 nm. Each of the samples was assessed three times. The equation (5) was used to determine the DPPH RSA of the samples.

$$DPPHRSA(\%) = \left(1 - \frac{A_1 - A_s}{A_0}\right) \times 100\% \quad (5)$$

A_1, As, and A_0 represent the absorbance of the sample, control, and blank, respectively, at 517 nm.

2.10.2. ABTS radical scavenging properties assay

ABTS RSA was studied using the same approach described by Zhan, Li, Dang, and Pan (2021). A 7.4 mmol/L ABTS solution and 2.6 mmol/L potassium persulfate solution were separately prepared. After that, potassium persulfate solution (88 mL) was mixed with 5 mL ABTS solution and subjected to incubation for 12–16 h. The resulting ABTS solution

was referred to as a working solution that was diluted with PBS buffer until the absorbance was 0.7 ± 0.02. Once the absorbance was adjusted to 0.7, 200 μL working solution was added to the sample (10 μL), and the resulting solution was subjected to incubation in the dark for 6 min followed by immediate determination of absorbance at 734 nm. The Eq. (6) was used to determine the ABTS RSA.

$$ABTSRSA(\%) = \left(\frac{A_0 - A_1}{A_0}\right) \times 100\% \quad (6)$$

A_1 and A_0 denote the absorbance of the sample and blank, respectively, at 734 nm.

2.11. Simulated digestion in the gastrointestinal tract (GIT)

As reported by Liu et al. (2022), a two-stage digestion method (in vitro) was employed to simulate human stomach and intestine conditions.

Stomach stage: The sample (5 mL) was mixed with 15 mL of simulated gastric fluid (SGF) containing pepsin and NaCl (3.2 and 2 mg/mL, respectively). Using a bath oscillator (JDS-BA, Jingda Instrument Co., Ltd., Changzhou, China) with constant temperature, the mixture was agitated for 2 h at 100 rpm and 37 °C after pH adjustment to a value of 2.0 with 1 mol/L HCl/NaOH.

Small intestine stage: The stomach stage solution (20 mL) was subjected to pH adjustment until 7.0 and then subsequently allowed to mix with a simulated intestinal fluid (SIF) composed of saline solution (CaCl2 and NaCl with the respective proportions of 36.7 and 218.7 mg/mL), lipase, 24 mg/mL pancreatin solution and 54 mg/mL bile salt solution. The pH-adjusted stomach solution was combined with SIF at a 1:1 (v/v) ratio. NaOH (0.1 mol/L) was added dropwise to the resultant liquid to maintain the pH at 7.0. A water bath oscillator with constant temperature was used to perform intestinal digestion of the mixture at 37 °C with continuous shaking for 2 h at 120 rpm. Using the pH-stat titration procedure, a constant pH of 7.0 was maintained via titration with NaOH (0.1 mol/L). The amount of NaOH consumed was recorded, and the equation (7) was used to determine the percentage of free fatty acids (FFAs%) at time.

$$FFAs(\%) = \frac{V_{NaOH(t)}C_{NaOH}M_{oil}}{2m_{oil}} \quad (7)$$

where $V_{NaOH(t)}$ represents the needed volume of NaOH (L) for the neutralization of FFAs at time, C_{NaOH} represents the concentration of NaOH (0.1 mol/L), and M_{oil} and m_{oil} represent the average MW of the oil (g/mol) and the initial lipid mass present in the reaction vessel, respectively.

2.12. Determination of astaxanthin content

The AST concentration in the emulsion systems was calculated using a slightly modified method developed by Boonlao, Shrestha, Sadiq, and Anal (2020). The emulsions (50 μL) were diluted in organic solvent (methanol: dichloromethane = 1:2, v/v, 4.95 mL) and then centrifuged at 4472g for 20 min. The AST concentration was determined in the supernatant by recording the absorbance at 480 nm. The AST-free emulsion served as a control. The AST standard was solubilized in organic solvent (methanol:dichloromethane = 1:2, v/v) throughout a concentration range of 0–12 mg/L, and a calibration curve was constructed.

2.13. In vitro bioaccessibility analysis

The AST digestion after in vitro digestion was measured using the method reported by Salvia-Trujillo, Qian, Martín-Belloso, and McClements (2013) after slight variation. Raw digesta (10 mL) was subjected to centrifugation at 716g for 60 min at 25 °C. The supernatant containing AST dissolved in a mixed micelle was collected after centrifugation.

Before analysing the micelle fraction, the top layer of undigested oil was removed. The 5 mL aliquots of raw digesta or micelle fraction were mixed with 5 mL organic solvent (methanol: dichloromethane = 1:2, v/v) followed by centrifugation at 137*g* for 10 min at 25 °C. The bottom layer containing AST was collected, while the top layer was mixed with 5 mL organic solvent, and the same protocol was repeated thrice. At 480 nm, the absorbance was determined after the bottom portion of the organic layer was combined with the previous one. The Eq. (8) was used to calculate AST digestion.

$$Astaxanthin digestion(\%) = 100 \times \left(\frac{C_{Micelle}}{C_{Rawdigesta}} \right) \tag{8}$$
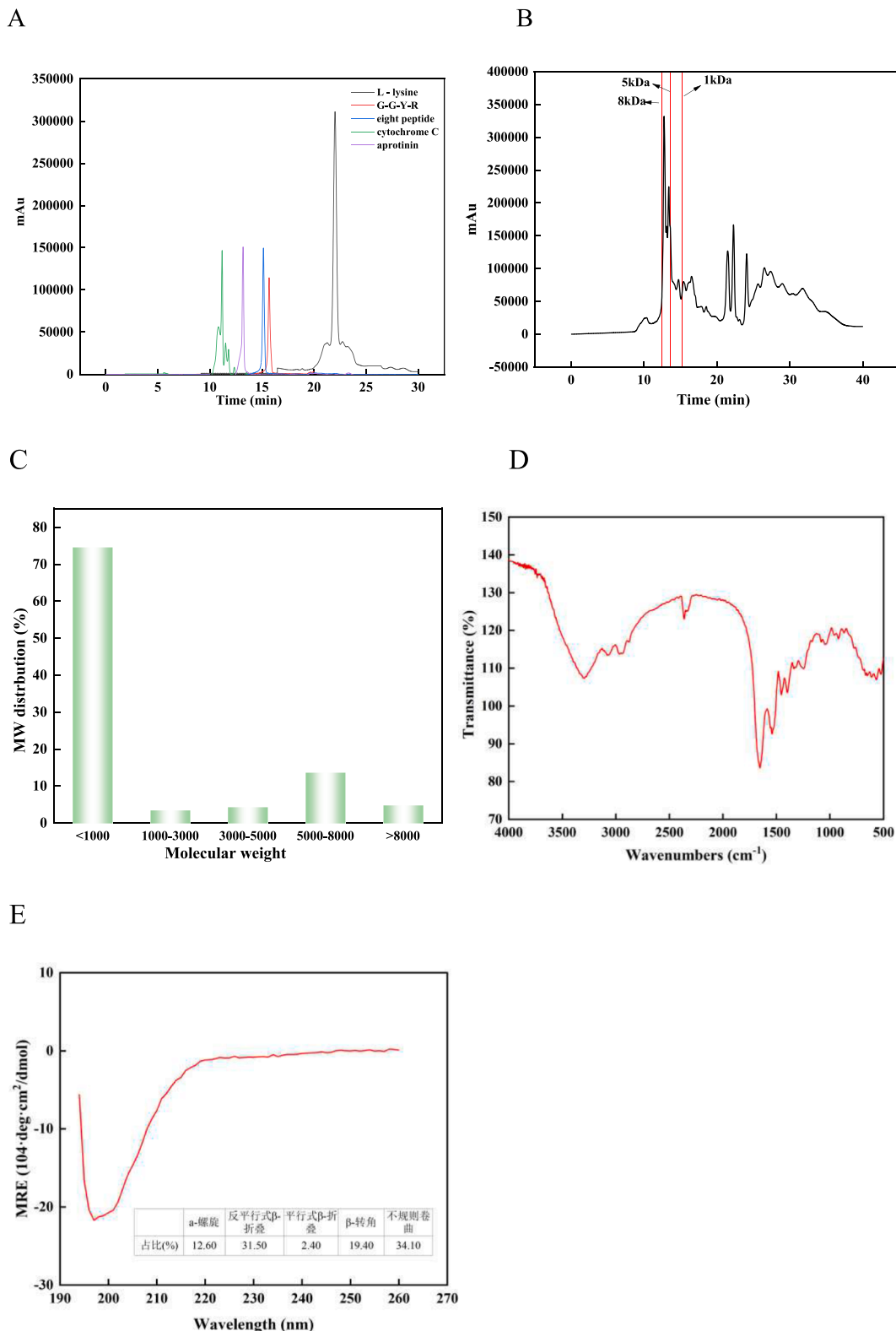

Fig. 1. A: Liquid chromatogram of the standard product and B: CSCP. C: Molecular weight distribution of CSCP. D: FTIR spectra of CSCP. E: CD spectrum of CSCP.

Here, $C_{Micelle}$ and C_{Raw} digesta represent the concentration of AST in the micelle fraction and raw digesta, respectively.

2.14. Statistical analysis

All experiments were performed in triplicate to obtain mean values, and the data are summarized as the mean $\pm$ standard deviation (SD). Significance analysis between groups was analyzed by one-way analysis of variance (ANOVA) and the significant difference analysis of data was represented by $p < 0.05$.

3. Results and discussions

3.1. Molecular structure of peptides

The peptide distribution results are presented in Fig. 1. The data showed that the CSCP sample contained a greater proportion of peptides with an MW of <1000 Da (74.5 %) than those with an MW of >1000 Da (25.5 %). The average CSCP MW was found to be 2146 Da. Fig. 1D displays the FTIR spectra of the CSCP. C═O and N—H stretching were represented by the CSCP peaks at 1652 cm^{-1} (amide I) and 1538 cm^{-1} (amide II), respectively. CD spectra were used to determine the secondary structure of proteins and their constituent parts. The CD spectrum (Fig. 1E) displayed a strong negative band at approximately 197 nm, representing the typical characteristic peak of a small peptide. CSCP contained 12.6 % α-helix, 33.9 % β-sheet, 19.4 % β-turn, and 34.1 %

random coil. The prevalence of irregularly curled structures in CSCP suggests that its structure is relatively porous and disordered.

3.2. Properties of Maillard reaction products

FT-IR spectroscopy is often used to analyse the secondary structure of proteins or polypeptides. It primarily analyses the structural changes of peptide chains through the typical characteristic peaks that appear in the mid-infrared region. Compared with native CSCP, the absorption peak of the ι-car-CSCP MRPs sugar conjugate was stronger in the range of 3000–3500 cm^{-1} owing to the bending vibration of the N—H bond or stretching vibration of the hydrogen bond, as shown in Fig. 2A. Furthermore, the Maillard reaction increased the stretching vibration of C—H, C—N, and C═O bonds, as demonstrated by an increase in the strength of the absorption peaks of the ι-car-CSCP MRPs between 1050 and 1100 cm^{-1}. The glycosylation products of ovalbumin and carboxymethylcellulose were prepared by Geng, who also reported the enhanced characteristic absorption peak of the hydroxyl group by FTIR (Geng et al., 2014). The results indicated that ι-car was covalently bound to the CSCP, leading to the formation of Maillard products.

The formation of Maillard reaction intermediates was monitored by measuring their UV absorbance (294 nm). To visually assess brown pigments in the last stage of the Maillard process, their browning intensity (420 nm) was determined. Fig. 2 illustrates the GD and browning intensity of the MRPs of ι-car-CSCP MRPs at various reaction times. Fig. 2B reveals the gradual increase in the GD value of ι-car-CSCP MRPs
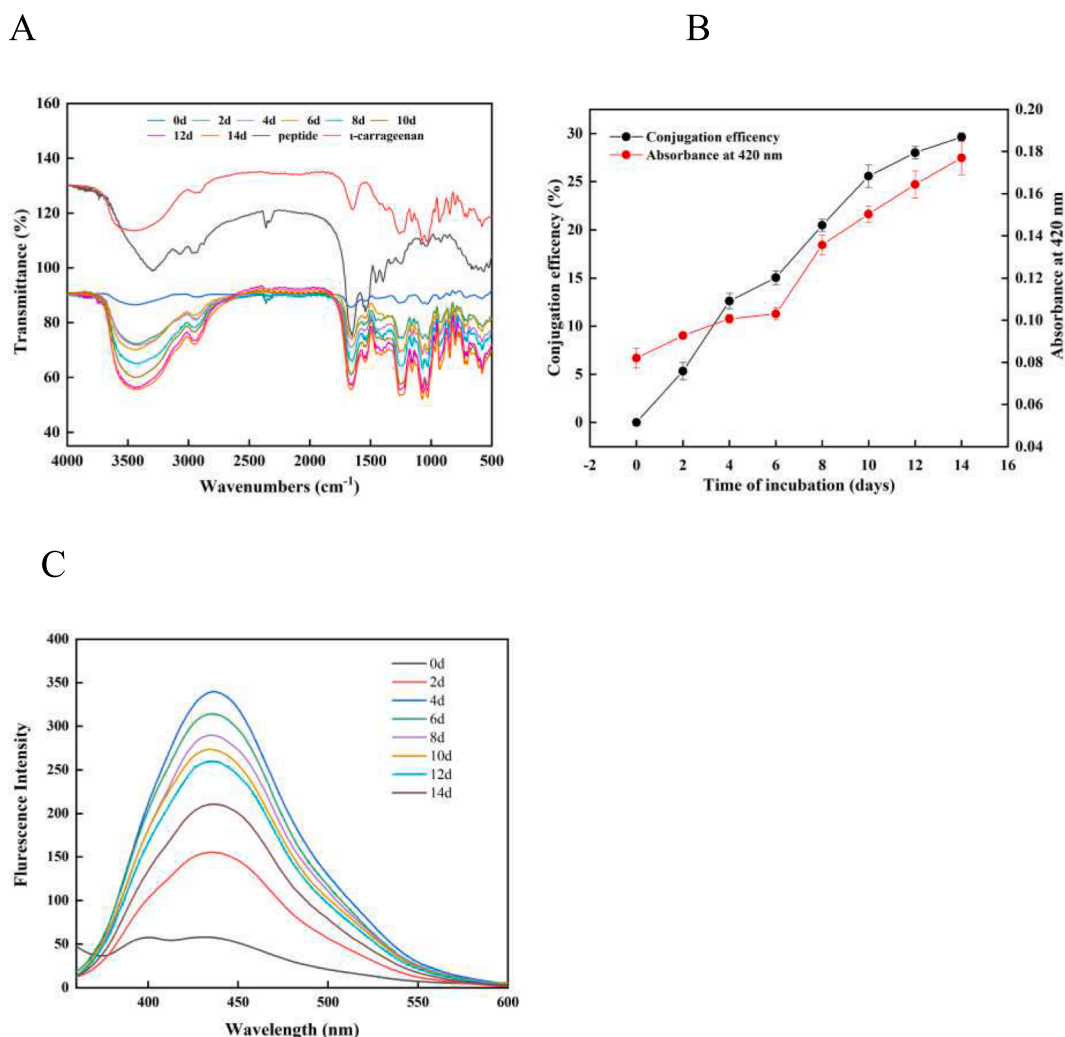
A

B

C

Fig. 2. A: FTIR spectra, B: Grafting rate and browning degree, and C: Fluorescence intensity of products at various reaction times.

with time, which reached a maximum after 14 d. Furthermore, Fig. 2 also shows the absorbance of the Maillard product at 420 nm at different reaction times. The results demonstrated a positive relationship between absorbance and reaction time, with higher absorbance values indicating a greater degree of browning. A similar result was also found in the previously reported whey protein-dextran system (Shi et al., 2019). This phenomenon was associated with the formation of a large number of brown polymer melanosomes at the late Maillard reaction stage. More pigment compounds were produced when the reaction time was increased, resulting in deeper browning.

Early indicators of the Maillard reaction include fluorescent chemicals, which were developed prior to the synthesis of browning products (Chen, Yang, Hong, Feng, Liu, & Luo, 2020). Strecker degradation during the Maillard reaction changed the initial intermediate into a noncolor fluorescent substance, and further reactions resulted in browning and the production of a fluorescent molecule, a precursor to the pigment material (Han et al., 2019). Fig. 2 exhibits the intrinsic fluorescence spectroscopy of ι-car-CSCP MRPs. The fluorescence intensity of ι-car-CSCP MRPs reached a maximum at 4 days, followed by a gradual decrease. Liu, Kong, Han, Sun, and Li (2014) observed similar results in glucose-whey protein isolate MRPs. They discovered that after 4 days, the fluorescence intensity of the glucose-whey protein isolate MRPs maximized before decreasing. A similar result was also reported in the ribose–casein system (Jing, & Kitts, 2002). This phenomenon may be caused by the destruction of the peptide chain structure during heating, which exposed more benzene rings with fluorescence absorption ability, thereby increasing the fluorescence intensity. However, after reaching the peak, the fluorescence intensity decreased with increasing reaction time, possibly due to the covalent reaction between peptide and carrageenan, which increased the steric hindrance of the reaction product and decreased the signal fluorescence absorbing amino acid, leading to a decrease in fluorescence intensity. Consequently, fluorescent substances were continually produced during the first 4 days, and after that, they were converted into brown compounds, resulting in a decrease in fluorescent substances and subsequent fluorescence intensity.

Scavenging free radicals is a fundamental mechanism for preventing lipid oxidation (McClements, & Decke, 2000). Chemical tests were conducted based on the compound's ability to scavenge DPPH and ABTS radicals, which represent model free radicals. Fig. 3A and 3B, respectively, display the DPPH and ABTS RSAs of MRPs on the CSCP and ι-car models, with findings expressed as percent scavenging on MRPs concentration of 1 mg/ml. The results showed that the DPPH and ABTS radical scavenging rates of MRPs were highest on the 10th day of incubation, with values of 27.91 ± 3.61 % and 25.67 ± 1.63 %,

respectively. This value was 18.19 % and 10.25 % higher than that of the mixture, which suggested that the Maillard reaction could contribute to increasing RSA. Antioxidant activity in MRPs, especially melanoidins, has been described by their ability to scavenge oxygen radicals or chelate metals (Yilmaz & Toledo, 2005). The current findings show that the best radical scavengers are not formed during the first stages of the Maillard reaction but rather develop after several days of heat treatment. Brown pigments of high MW form during prolonged treatment; these pigments are partially insoluble and could impede the detection of antiradical behaviour (Maillard, Billaud, Chow, Ordonaud, & Nicolas, 2007).

3.3. Effect of Maillard reaction on preparation of emulsion

EAI and ESI were used to examine the emulsifying ability of glycosylated proteins. Fig. 4 reflects the EAI and ESI of ι-car-CSCP MRPs at various reaction times. The EAI and ESI of conjugates were, as predicted, significantly higher than those of ι-car-CSCP because ι-car was covalently attached to a protein to form a macromolecular stabilizing layer around oil droplets and stabilize them against creaming, coalescence and flocculation (Chen et al., 2019). As expected, the increase in reaction time resulted in an initial increase in the emulsifying potential, which subsequently decreased. Furthermore, ι-car-CSCP MRPs reached the maximum EAI and ESI at 10 days following the reaction, with 64.10 ± 3.14 m^2/g and 111.99 ± 7.18 min, respectively. It is now well understood that protein-saccharide conjugation results in the combination of distinctive features of proteins and saccharides. The EAI and ESI of proteins were enhanced because the hydrophobic protein bound to the oil droplet surface and the hydrophilic group of the covalently connected saccharide was absorbed, conferring colloidal stability by thickening the water phase during emulsification (Chailangka et al., 2022). Prolonged exposure causes the sample to turn brown, which reduces protein solubility and causes damage, leading to reduced absorption at the interface layer and decreasing the emulsion's stability (Xu, Wang, Jiang, Yuan, & Gao, 2012). The observed result was similar to that reported by Xiao, Woo, Hu, Xiong, and Zhao (2021). It was discovered that the emulsifying ability of protein hydrolysates was enhanced by the presence of enzyme-hydrolysed rice protein-glucose MRPs, where EAI initially increased and subsequently decreased with elongation reaction time.

FFAs from the MRPs-AKO emulsion were liberated throughout time during the digestive process at all phases, implying the release of AST into the system. Fig. 4A depicts FFAs released by the emulsions after digestion in the small intestine. The lipid digestion patterns of the seven
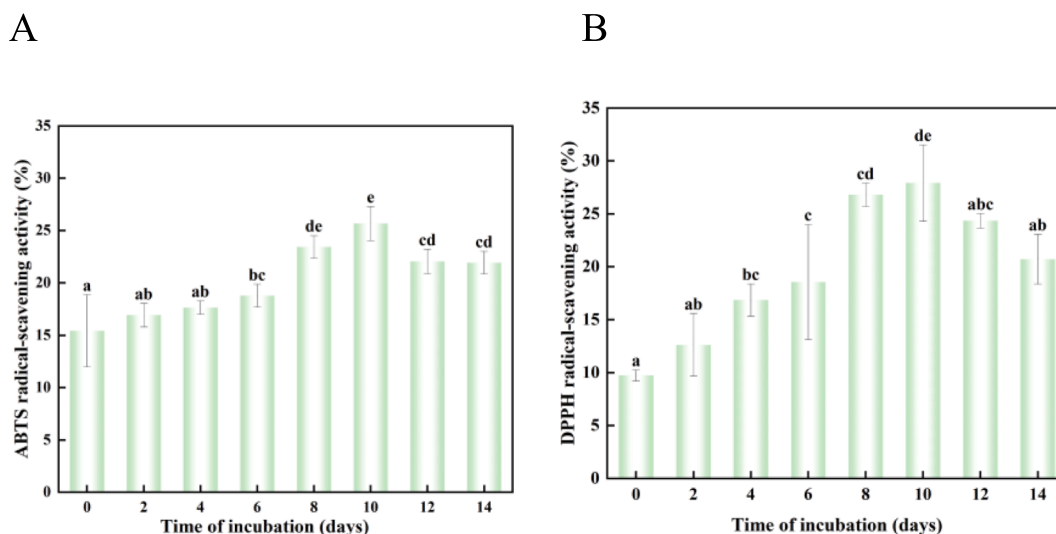
A

B

Fig. 3. A: ABTS RSA and B: DPPH RSA of ι-car-CSCP MRPs at different reaction times.
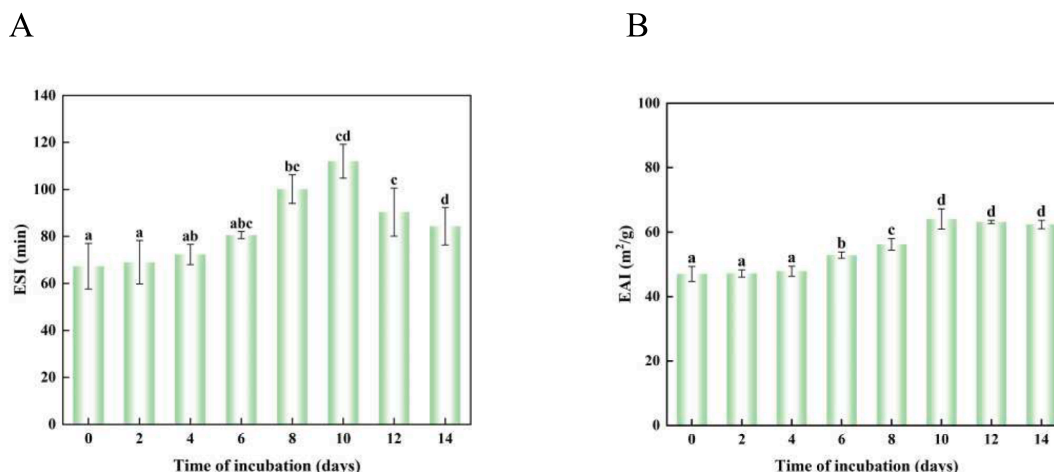
A

B

Fig. 4. A: Emulsifying activity index and B: Emulsifying stability index of ι-car-CSCP MRPs at different reaction times.

emulsions followed a similar pattern. The FFAs in the seven emulsions increased dramatically in the first 20 min and then varied slowly until 120 min of digestion. The results were comparable with those of Liu et al. (2022). These findings suggest that the emulsion structure was partially degraded during digestion in the stomach and that AKO was partially exuded and reacted with pancreatic enzymes and bile salts in the intestine. Throughout digestion, it was discovered that the ultimate rate and extent of lipid digestion (FFAs release) were greater in the 10d-MRPs-AKO emulsion than in the other MRPs-AKO emulsions.

Overall bioaccessibility after digestion is represented by the fraction of AST that is solubilized in the mixed-micelle phase (Chitindingu, Benhura, & Muchuweti, 2015). The bioaccessibility of AST in the MRP-AKO emulsion was evaluated after a simulation of GIT digestion. The results demonstrated that the bioavailability of AST in MRPs-AKO remained essentially constant following the initial increase with increasing reaction time (Fig. 5). The lotion containing MRPs that had been incubated for 10 days had the highest bioavailability of AST of 28.48 %. This may be associated with the good emulsification of the Maillard-modified peptide and the smaller emulsion size. It has been suggested that MRPs have a role in limiting droplet aggregation during in vitro examinations of intestinal digestion, which in turn improves lipase access to the droplet surface. Meanwhile, the smaller emulsion inhibits droplet aggregation during digestion, accelerates the degradation of the oil phase, and promotes AST bioaccessibility (Shi, Ye, Zhu, & Miao, 2022). Furthermore, the fat release in the emulsion exhibited a similar trend to the bioavailability of AST (Fig. 4A and B), which is

consistent with the findings observed by Salvia-Trujillo, Qian, Martin-Belloso, and McClements (2013). It was speculated that MRPs lotion can maintain the controlled release of AST by regulating the fat content in gastric juice.

Secondary and primary oxidation products formed over 30 days of light-protected storage at 25 °C were used to assess the eight emulsions' oxidative stability. With increasing oxidation time, the content of hydroperoxide increased in the control and four emulsions, indicating a gradual decrease in the oxidative stability of the oil, as shown in Fig. 6. Since the oils were oxidized due to shear pressures and other causes throughout the emulsion production process, the content of hydroperoxide of the emulsions embedded in the initial state was higher compared with the control group AKO. However, by Day 6, the control group had surpassed the oxidation rate of the oils incorporated in the emulsion. After 30 days, the concentration of hydroperoxide was 43.58 mmol/kg, while it was 37.24, 36.18, 35.91, 32.13, 29.48, 30.10, and 30.51 mmol/kg in the eight emulsions. All of these values were significantly lower than the concentration in native AKO (P < 0.05). In addition, the lotion prepared by ι-car-CSCP MRPs exhibited the lowest POV value after incubation for 10 days.

TBARS results are among the indicators used to distinguish lipid secondary oxidation. Typically, they are employed in conjunction with hydroperoxides to describe the oxidation process of lipids. According to Fig. 6B, the TBARs value of AKO and lotion increased slowly before Day 6, and the increase rate was accelerated after 6 days, possibly owing to the breakdown of the primary product of lipid preoxidation into the
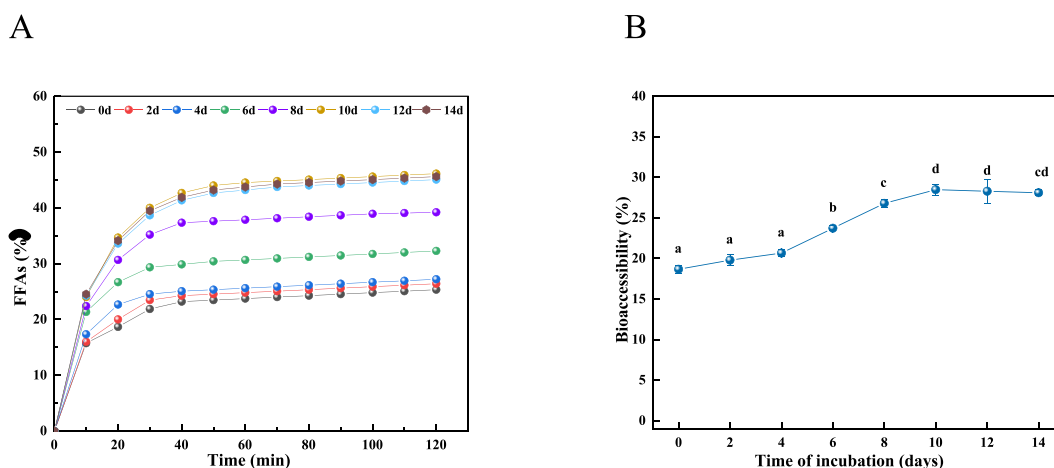
A

B

Fig. 5. A: The release of FFAs and B: bioaccessibility of quercetin in the stabilized emulsions.
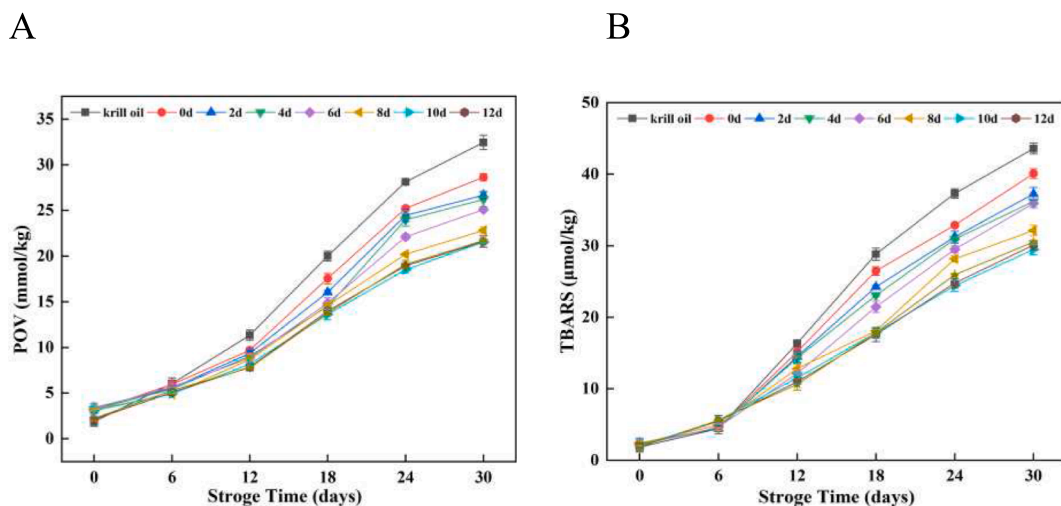
A

B

Fig. 6. A: Peroxide values and B: TBAR values of AKO emulsions stabilized by ι-car-CSCP MRPs at different reaction times.

secondary product. After 6 days, the TBARS value of AKO was greater than that of lotion prepared by the product, whose value was lowest even on the 14th day. The results revealed that the antioxidant properties of the lotion prepared by the Maillard reaction were significantly improved during storage. This was due to the Maillard reaction producing active compounds such as melanoids, which can eliminate free radicals and chelate metal ions, hence delaying the oxidation of oils.

4. Conclusions

This study reported the preparation of antioxidant emulsifiers using the Maillard reaction by conjugating CSCP and ι-car. The MRPS conjugates prepared from ι-car and CSCP produced antioxidant substances such as melanins, which further enhanced the antioxidant potential. Simultaneously, the emulsifying properties of MRPs were improved, with suitable DG (25.58 %), preventing the oxidation of AKO emulsion and ensuring the emulsion quality, making it able to be adsorbed on the AKO droplet surface, hence serving as a good stabilizer for oil emulsion. Meanwhile, in vitro digestibility indicated the highest FFA release of the AKO emulsion by MRPs incubated for 10 days with DG at 25.58 % and 28.48 % of the highest bioavailability of AST in the MRPs-AKO emulsion from the lotion prepared by MRPs after incubation for 10 days. This research could have implications for the development of emulsified foods that include polyunsaturated lipids with health benefits.

CRediT authorship contribution statement

Lingyu Han: Conceptualization, Investigation, Methodology, Writing – original draft. **Ruiyi Zhai:** Investigation, Methodology, Writing – original draft, Writing – review & editing. **Ruitao Shi:** Investigation, Methodology, Writing – original draft. **Bing Hu:** Conceptualization, Formal analysis, Methodology, Writing – review & editing. **Jixin Yang:** Conceptualization, Methodology, Writing – review & editing. **Zhe Xu:** Methodology, Writing – review & editing. **Kun Ma:** Software, Validation, Writing – review & editing. **Yingmei Li:** Visualization, Writing – review & editing. **Tingting Li:** Methodology, Writing – original draft, Writing – review & editing.

Declaration of competing interest

The authors declare that they have no known competing financial interests or personal relationships that could have appeared to influence the work reported in this paper.

Data availability

No data was used for the research described in the article.

References

Abdelhedi, O., & Nasri, M. (2019). Basic and recent advances in marine antihypertensive peptides: Production, structure-activity relationship and bioavailability. *Food Chemistry, 88*, 543–557. https://doi.org/10.1016/j.tifs.2019.04.002

Ai, M., Xiao, N., & Jiang, A. (2021). Molecular structural modification of duck egg white protein conjugates with monosaccharides for improving emulsifying capacity. *Food Hydrocolloids, 111*, Article 106271. https://doi.org/10.1016/j.foodhyd.2020.106271

Bakry, A. M., Abbas, S., Ali, B., Majeed, H., Abouelwafa, M. Y., Mousa, A., & Liang, L. (2016). Microencapsulation of oils: A comprehensive review of benefits, techniques, and applications. *Comprehensive Reviews in Food Science and Food Safety, 15*(1), 143–182. https://doi.org/10.1111/1541-4337.12179

Berton-Carabin, C. C., Ropers, M. H., & Genot, C. (2014). Lipid oxidation in oil-in-water emulsions: Involvement of the interfacial layer. *Comprehensive Reviews in Food Science and Food Safety, 13*(5), 945–977. https://doi.org/10.1111/1541-4337.12097

Boonlao, N., Shrestha, S., Sadiq, M. B., & Anal, A. K. (2020). Influence of whey protein-xanthan gum stabilized emulsion on stability and in vitro digestibility of encapsulated astaxanthin. *Journal of Food Engineering, 272*, Article 109859. https://doi.org/10.1016/j.jfoodeng.2019.109859

Cao, J., Yan, H., & Liu, L. (2022). Optimized preparation and antioxidant activity of glucose-lysine Maillard reaction products. *LWT - Food Science and Technology, 161*, Article 113343. https://doi.org/10.1016/j.lwt.2022.113343

Chailangka, A., Seesuriyachan, P., Wangtueai, S., Ruksiriwanich, W., Jantanasakulwong, K., Rachtanapun, P., Phimolsiripol, Y., Sommano, S. R., Leksawasdi, N., Barba, F. J., & Phimolsiripol, Y. (2022). Cricket protein conjugated with different degrees of polymerization saccharides by Maillard reaction as a novel functional ingredient. *Food Chemistry, 395*, Article 133594. https://doi.org/10.1016/j.foodchem.2022.133594

Chen, K., Yang, Q., Hong, H., Feng, L., Liu, J., & Luo, Y. (2020). Physicochemical and functional properties of Maillard reaction products derived from cod (Gadus morhua L.) skin collagen peptides and xylose. *Food Chemistry, 333*, Article 127489. https://doi.org/10.1016/j.foodchem.2020.127489

Chen, W. J., Ma, X. B., Wang, W. J., Lv, R. L., Guo, M. M., Ding, T., Ye, X. Q., Miao, S., & Liu, D. H. (2019). Preparation of modified whey protein isolate with gum acacia by ultrasound Maillard reaction. *Food Hydrocolloids, 95*, 298–307. https://doi.org/10.1016/j.foodhyd.2018.10.030

Chitindingu, K., Benhura, M. A. N., & Muchuweti, M. (2015). In vitro bioaccessibility assessment of phenolic compounds from selected cereal grains: A prediction tool of

nutritional efficiency. *LWT - Food Science and Technology, 63*(1), 575–581. https://doi.org/10.1016/j.lwt.2015.02.026

El-Messery, T. M., Altuntas, U., Altin, G., & Özçelik, U. (2020). The effect of spray-drying and freeze-drying on encapsulation efficiency, in vitro bioaccessibility and oxidative stability of krill oil nanoemulsion system. *Food Hydrocolloids, 106*, Article 105890. https://doi.org/10.1016/j.foodhyd.2020.105890

Geng, X., Cui, B., Li, Y., Jin, W., An, Y., Zhou, B., & Li, B. (2014). Preparation and characterization of ovalbumin and carboxymethyl cellulose conjugates via glycosylation. *Food Hydrocolloids, 37*, 86–92. https://doi.org/10.1016/j.foodhyd.2013.10.027

Han, Y. T., Zhao, C. C., Han, J. R., Yan, J. N., Du, Y. N., Shang, W. H., & Wu, H. T. (2019). Antioxidant activity of sea cucumber (Stichopus japonicus) gut hydrolysates-ribose Maillard reaction products derived from organic reagent extraction. *Journal of Food Measurement and Characterization, 13*(4), 2790–2797. https://doi.org/10.1007/s11694-019-00199-0

Hong, H., Fan, H., Chalamaiah, M., & Wu, J. (2019). Preparation of low-molecular-weight, collagen hydrolysates (peptides): Current progress, challenges, and future perspectives. *Food Chemistry, 301*, Article 125222. https://doi.org/10.1016/j.foodchem.2019.125222

Hwang, I. G., Kim, H. Y., Woo, K. S., Lee, J. S., & Jeong, H. S. (2011). Biological activities of Maillard reaction products (MRPs) in a sugar–amino acid model system. *Food Chemistry, 126*, 221–227. https://doi.org/10.1016/j.foodchem.2010.10.103

Jing, H., & Kitts, D. D. (2002). Chemical and biochemical properties of casein–sugar Maillard reaction products. *Food and Chemical Toxicology, 40*(7), 1007–1015. https://doi.org/10.1016/S0278-6915(02)00070-4

Liu, G., Hu, M., Du, X., Yan, S., Liao, Y., Zhang, S., & Li, Y. (2022). Effects of succinylation and chitosan assembly at the interface layer on the stability and digestion characteristics of soy protein isolate-stabilized quercetin emulsions. *LWT - Food Science and Technology, 154*, Article 112812. https://doi.org/10.1016/j.lwt.2021.112812

Liu, Q., Kong, B., Han, J., Sun, C., & Li, P. (2014). Structure and antioxidant activity of whey protein isolate conjugated with glucose via the Maillard reaction under dry-heating conditions. *Food Structure, 1*(2), 145–154. https://doi.org/10.1016/j.foostr.2013.11.004

Maillard, M. N., Billaud, C., Chow, Y. N., Ordonaud, C., & Nicolas, J. (2007). Free radical scavenging, inhibition of polyphenoloxidase activity and copper chelating properties of model Maillard systems. *LWT- Food Science and Technology, 40*, 1434–1444. https://doi.org/10.1016/j.lwt.2006.09.007

Mao, L., Pan, Q., Hou, Z., Yuan, F., & Gao, Y. (2018). Development of soy protein isolate-carrageenan conjugates through Maillard reaction for the microencapsulation of Bifidobacterium longum. *Food Hydrocolloids, 84*, 489–497. https://doi.org/10.1016/j.foodhyd.2018.06.037

McClements, D. J., & Decke, E. A. (2000). Lipid oxidation in oil-in-water emulsions: Impact of molecular environment on chemical reactions in heterogeneous food systems. *Journal of Food Science, 65*(8), 1270–1282. https://doi.org/10.1111/j.1365-2621.2000.tb10596.x

Morales, F. J., & Babbel, M. B. (2002). Antiradical efficiency of Maillard reaction mixtures in a hydrophilic media. *Journal of Agricultural and Food Chemistry, 50*, 2788–2792.

Nagachinta, S., & Akoh, C. C. (2013). Spray-dried structured lipid containing long-chain polyunsaturated fatty acids for use in infant formulas. *Journal of Food Science, 78* (10), 1523–1528. https://doi.org/10.1111/1750-3841.12243

Olmedo, R., Nepote, V., & Grosso, N. R. (2014). Antioxidant activity of fractions from oregano essential oils obtained by molecular distillation. *Food Chemistry, 156*, 212–219. https://doi.org/10.1016/j.foodchem.2014.01.087

Salvia-Trujillo, L., Qian, C., Martin-Belloso, O., & McClements, D. J. (2013). Influence of particle size on lipid digestion and beta-carotene bioaccessibility in emulsions and nanoemulsions. *Food Chemistry, 141*(2), 1472–1480. https://doi.org/10.1016/j.foodchem.2013.03.050

Sánchez, O. C. A., Bonilla, Z. E., Urrea, G. G. R., Solano, L. G., & Rascón, D. M. P. (2021). Krill oil microencapsulation: Antioxidant activity, astaxanthin retention, encapsulation efficiency, fatty acids profile, in vitro bioaccessibility and storage stability. *LWT - Food Science and Technology, 147*, Article 111476. https://doi.org/10.1016/j.lwt.2021.111476

Shi, Y., Liang, R., Chen, L., Liu, H., Goff, H. D., Ma, J., & Zhong, F. (2019). The antioxidant mechanism of Maillard reaction products in oil-in-water emulsion system. *Food Hydrocolloids, 87*, 582–592. https://doi.org/10.1016/j.foodhyd.2018.08.039

Shi, Y., Ye, F., Zhu, Y., & Miao, M. (2022). Development of dendrimer-like glucan-stabilized Pickering emulsions incorporated with beta-carotene. *Food Chemistry, 385*, Article 132626. https://doi.org/10.1016/j.foodchem.2022.132626

Siewe, F. B., Kudre, T. G., Bettadaiah, B. K., & Narayan, B. (2020). Effects of ultrasound-assisted heating on aroma profile, peptide structure, peptide molecular weight, antioxidant activities and sensory characteristics of natural fish flavouring. *Ultrason Sonochem, 65*, Article 105055. https://doi.org/10.1016/j.ultsonch.2020.105055

Wang, C., Sun, C., Lu, W., Gul, K., Mata, A., & Fang, Y. (2020). Emulsion structure design for improving the oxidative stability of polyunsaturated fatty acids. *Comprehensive Reviews in Food Science and Food Safety, 19*(6), 2955–2971. https://doi.org/10.1111/1541-4337.12621

Xiao, Q., Woo, M. W., Hu, J., Xiong, H., & Zhao, Q. (2021). The role of heating time on the characteristics, functional properties and antioxidant activity of enzyme-hydrolyzed rice proteins-glucose Maillard reaction products. *Food Bioscience, 43*. https://doi.org/10.1016/j.fbio.2021.101225

Xie, D., Gong, M., Wei, W., Jin, J., Wang, X., Wang, X., & Jin, Q. (2019). Antarctic krill (Euphausia superba) oil: A comprehensive review of chemical composition, extraction technologies, health benefits, and current applications. *Comprehensive Reviews in Food Science and Food Safety, 18*(2), 514–534. https://doi.org/10.1111/1541-4337.12427

Xu, D., Wang, X., Jiang, J., Yuan, F., & Gao, Y. (2012). Impact of whey protein – Beet pectin conjugation on the physicochemical stability of β-carotene emulsions. *Food Hydrocolloids, 28*(2), 258–266. https://doi.org/10.1016/j.foodhyd.2012.01.002

Yilmaz, Y., & Toledo, R. (2005). Antioxidant activity of water-soluble Maillard reaction products. *Food Chemistry, 93*(2), 273–278. https://doi.org/10.1016/j.foodchem.2004.09.043

Yu, M., He, S., Tang, M., Zhang, Z., Zhu, Y., & Sun, H. (2018). Antioxidant activity and sensory characteristics of Maillard reaction products derived from different peptide fractions of soybean meal hydrolysate. *Food Chemistry, 243*, 249–257. https://doi.org/10.1016/j.foodchem.2017.09.139

Zhan, J., Li, G., Dang, Y., & Pan, D. (2021). Study on the antioxidant activity of peptide isolated from porcine plasma during in vitro digestion. *Food Bioscience, 42*, Article 101069. https://doi.org/10.1016/j.fbio.2021.101069